Available on CMS information server

CMS NOTE -2009/008

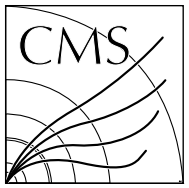

The Compact Muon Solenoid Experiment

CMS Note

Mailing address: CMS CERN, CH-1211 GENEVA 23, Switzerland

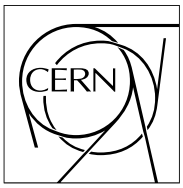

08 February 2008 (v2, 06 April 2009)

Local Muon Reconstruction in the Drift Tube Detectors

N. Amapane[1)], R. Bellan[1)2)], S. Bolognesi[1)2)], G. Cerminara[3)], S. Lacaprara[4)], M. Pelliccioni[1)].

Abstract

This note describes the local reconstruction in the Drift Tube subdetector of the CMS muon subsystem. The local reconstruction is the sequence of steps leading from the TDC measurements to reconstructed three-dimensional segments inside each DT chamber. These segments are the input to the muon track reconstruction. This note updates and supersedes CMS NOTE 2002/043

[1)] Università di Torino e Sezione dell'INFN, Torino, Italy

[2)] Now at CERN, Geneva, Switzerland

[3)] INFN Torino, Italy

[4)] INFN Legnaro National Laboratory, Italy

1 Introduction

The main purpose of this note is to describe the local reconstruction in the CMS Drift Tube (DT) detectors. This is the reconstruction step where basic hits and track segments in a chamber are built starting from the output of the Data Acquisition System.

Local reconstruction begins with the reconstruction of mono-dimensional hits in single drift cells. The only information contained in these hits is their distance from the wire, with an intrinsic left/right ambiguity and without any information about their position along the tube.

The cell hits are the basic ingredients for the reconstruction of segments in the r-ϕ and r-z projections separately. These two-dimensional segments still do not provide any information about the coordinate parallel to the sense wires, but they measure the track angle in the measurement plane (orthogonal to the wires).

By combining the two projections, it is possible to reconstruct the three-dimensional information about the muon traversing the chamber. The resulting three-dimensional segments are the input to the muon track fit in the CMS spectrometer both in the offline and in the High Level Trigger reconstruction. The performance of the reconstruction must therefore meet the reliability and robustness requirements needed by such a task: provide good resolution on the track position and direction with a limited processing time, even in a high multiplicity environment.

In the following, after a brief description of the CMS Muon System and a detailed overview of the DT design (Section 2), all the steps leading to the reconstruction of three-dimensional segments within the chambers, starting from the TDC measurements, are described (Section 4 and 5). The performance of each step is also discussed, focusing mainly on resolution.

All the algorithms presented in this note have been implemented in CMSSW [1], the official reconstruction software package of the CMS experiment.

2 The CMS Muon System

The CMS [2] design was driven by the requirement of a robust and redundant muon system. The muon spectrometer [3] is composed of three independent subsystems, which are all used both for tracking and trigger purposes in order to guarantee robustness and redundancy. The layout of the system is shown in Fig. 1.

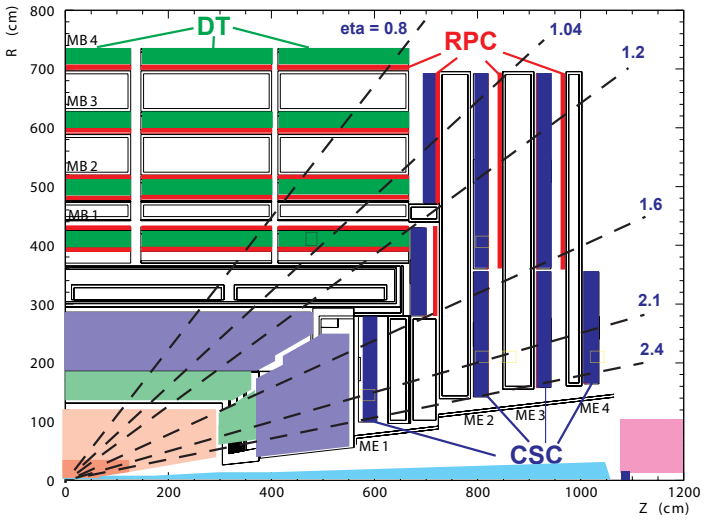

Figure 1: Longitudinal view of one quarter of the muon system.

In the barrel region ($|\eta| < 1.2$), where both track occupancy and residual magnetic field are low, drift tube detectors (DT) are installed.

In the endcaps the particle rate is higher and a large residual magnetic field is present. For this reason cathode strip chambers (CSC) are employed.

The combination of the DT and the CSC system covers the region $|\eta| < 2.4$. A third system, composed of resistive plate chambers (RPC), is installed up to $|\eta| < 1.6$, with a future extension planned to cover up to $|\eta| < 2.1$. RPCs are characterized by a limited spatial resolution but an excellent time resolution and fast response, thus providing unambiguous bunch crossing identification.

The muon identification is guaranteed by the amount of material upstream of the chambers and in the return yoke of the magnet, which shields the spectrometer from charged particles other than muons. More than 10 interaction lengths and 110 radiation lengths are present before the first measurement station of the spectrometer.

The magnetic field inside the iron of the yoke bends the tracks in the transverse plane thus allowing the measurement of their transverse momentum (p_T). The high field is fundamental for the momentum resolution of the spectrometer but it also sets the environment in which the detector operates. In the barrel region most of the flux is contained within the iron plates of the yoke, where the axial component of the field reaches ≈ 1.8 T. The space where the DT chambers are placed should ideally be field-free; however in the iron gaps and at the end of the coil the residual magnetic field is far from negligible. There are spatially limited regions where the field in the radial direction can reach 0.8 T [4].

2.1 The Barrel Drift Tube Chambers

The basic element of a DT detector is the drift cell, whose section is shown in Fig. 2. A layer of cells is obtained

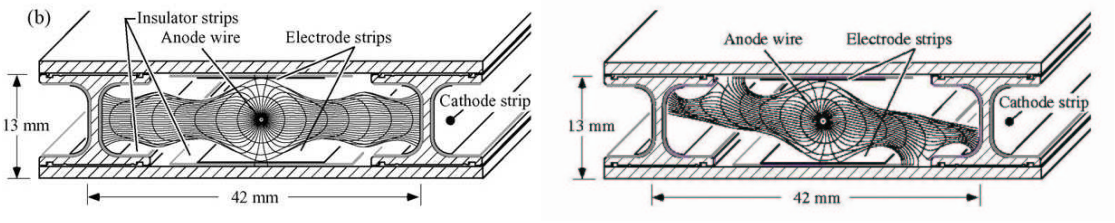

Figure 2: Transverse view of a Drift Tube cell in the barrel. The drift lines and the isochrones for a typical voltage configuration of the electrodes and representative gas mixture are shown for the case of zero magnetic field (left) and a 0.45 T magnetic field parallel to the anode wires (right).

by two parallel aluminium planes separated by "I"-shaped aluminium beams which define the boundary of the cells. The cell has a transverse size of 42×13 mm^2 with a 50 μm diameter stainless steel anode wire at the centre. The distance of the track from the wire is given by the drift time of electrons produced by ionization; to improve the distance-time linearity, additional field shaping is obtained with two positively-biased insulated strips, glued on the planes matching the wire position. Typical operational voltages are +3600 V, +1800 V and -1200 V for the wires, the strips and the cathodes, respectively. The gas is a $85\%/15\%$ mixture of Ar/CO_2, which provides good quenching properties and a saturated drift velocity of about 54 μm/ns. The maximum drift time is therefore ≈ 390 ns, i.e. 15 bunch crossings. A single cell has an efficiency of about 99.8% and a spatial resolution of about 180 μm [5].

Four staggered layers of parallel cells form a *superlayer*, which provides the measurement of two-dimensional segments thus solving the left-right ambiguity of a single layer. Also, the information of a superlayer is used by the trigger to identify the bunch crossing to which segment corresponds with no need of external input, using a generalization of the mean-timer technique [6].

A chamber is composed by two superlayers measuring the r-ϕ coordinates, with the wires parallel to the beam line, and an orthogonal superlayer measuring the r-z coordinates. The latter is not present in the outermost station (MB4). The wire length varies, depending on the superlayer type and on the station, from about 2 m to 3 m. The superlayers are glued on the two sides of an honeycomb spacer which ensures a ≈ 25 cm long lever arm for the measurement in the r-ϕ bending plane, as well as the required stiffness to the structure. A schematic view of a chamber is shown in Fig. 3.

The wires in each superlayer receieve the high voltage on one side ("HV side") and are read out on the other side ("front-end side"). The Level-1 local trigger and read-out electronics [7] is placed on the chamber, in a Mini-Crate (MC) mounted on the front-end side of the r-ϕ superlayers, inside a "C" profile surrounding the honeycomb structure.

2.1.1 Labeling and Reference Frames

The chamber segmentation follows that of the iron yoke, consisting of five wheels along the z axis, each divided into 12 azimuthal sectors. The wheels are numbered from -2 to +2, sorted according to global CMS z axis, with wheel 0 situated in the central region around $\eta = 0$.

Within each wheel, chambers are arranged in four *stations* at different radii and are named MB1, MB2, MB3 and MB4 as shown in Fig. 1. The first and the fourth station are mounted on the inner and outer face of the yoke, respectively; the remaining two are installed in slots within the iron plates.

In each wheel, a station consists of 12 chambers, one per sector, except for MB4 where 14 chambers are present. Sector numbering increases counter-clockwise when looking at the detector from the positive z axis, starting from sector number 1 which contains the vertical chambers matching the positive x axis in the CMS global reference frame. The additional two chambers in MB4 are numbered 13 and 14 according to the scheme shown in Fig. 4.

The convention on chamber numbering and local reference frames used in the CMS simulation and reconstruction software is shown in Figures 3 and 4.

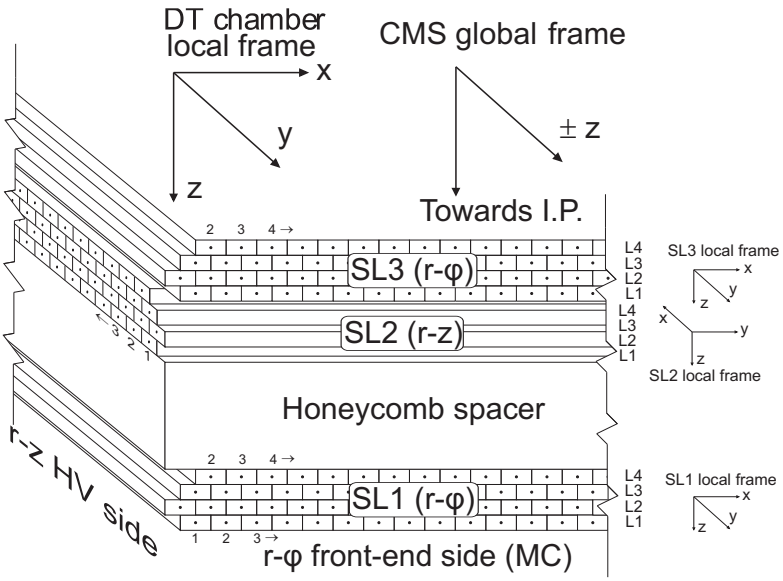

Figure 3: Schematic view of a DT chamber, showing the conventions on superlayer, layer and wire numbering and the orientation of reference frames.

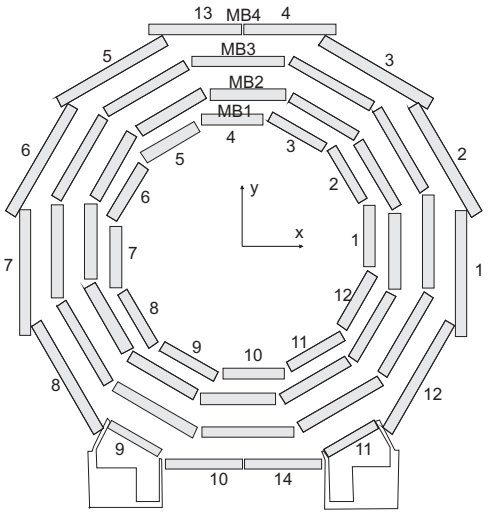

Figure 4: Numbering of stations and sectors.

Superlayers are numbered from 1 (innermost r-ϕ) to 3 (outermost r-ϕ). Number 2 is thus always the r-z superlayer, when present.

Layers are numbered from 1 (innermost) to 4 (outermost). A local reference frame is associated to each layer; the origin is placed at the centre of the layer, the x axis along the measured coordinate and the y axis along the wires, pointing towards the superlayer's front-end side). Cell number increases with increasing x.

Superlayers have a local reference frame oriented in the same way as the layers, but with the origin at the superlayer centre.

The chamber reference frame has the origin in the chamber centre and is oriented as the r-ϕ superlayer reference frames, i.e. with the x axis along the coordinate measured by the r-ϕ superlayers and the y axis along the coordinate measured by the r-z superlayer, pointing towards the r-ϕ front-end side.

With this choice of reference frames, the z axis of all local reference frames points toward the interaction region.

Chambers are installed in CMS with the front-end of r-ϕ superlayers in the side farther from the interaction point (i.e. with the chamber y axis pointing outwards). This allows a rough compensation, in r-ϕ superlayers, of the different time of flight of particles at different η with the propagation time along the wires. In wheel 0, chambers in pairs of neighboring serctors are installed with opposite orientation. The chamber local reference frames are oriented accordingly: in positive wheels (+1, +2) the chamber y axes are oriented along the global CMS z axis, while in negative wheels the x axis points towards the opposite direction.

3 Input to the Local Reconstruction

The input to the local reconstruction are TDC measurements stored in the so-called "digis". During data taking the DT digis are created by decoding ("unpacking") the raw output of the Data Acquisition (DAQ) system. In case of simulated samples, the digis are created by the digitization procedure [4], starting from the hits generated in the cell volume by the GEANT simulation. In both cases, the time measurement contained in a digi is not only the drift time of ionization electrons in the cell, but also contains other contributions:

- the time-of-flight (TOF) of the muon from the interaction point to the cell;
- the propagation time of the signal along the anode wire;
- delays due to the cable length and read-out electronics;
- the latency of the Level-1 trigger.

A synchronization procedure must therefore be applied to the digis in order to extract the drift time, which is the relevant information for hit reconstruction. This procedure must be flexible enough to fit different running conditions, such as cosmic ray data, test beams, and p–p collisions. A full description of this synchronization procedure is presented elsewhere [8] and is briefly summarized in this section.

First, the difference of the signal path lengths from each wire to the readout electronics is corrected within a chamber. This difference, called t_0, is measured for each wire by sending simultaneous "test-pulses" to the front-ends and computing the difference between the measured times and a reference value, taken as the average of all the channels in a chamber.

Once wires within a chamber are synchronized, the absolute time pedestal, called $t_{\rm trig}$, is computed from the distribution of drift times using the procedure described in [8].

The $t_{\rm trig}$ is normally computed for each superlayer separately. It accounts for the TOF and signal propagation along the wire, averaged on the tracks used in the calibration procedure. Further corrections for these two averages can be computed as soon as the three-dimensional hit position within the chamber is known, i.e. when the hit is included in a three-dimensional segment. In the case of p–p collisions, the chamber illumination is approximately uniform and the averages of TOF and signal propagation time correspond to the values of these quantities for a muon crossing the superlayer centre. The following corrections are therefore applied:

- the hit position is used to correct for the difference in the TOF of an infinite-momentum particle crossing the superlayer centre and one traveling to the actual hit position;
- the hit coordinate along the wire is used to correct for the propagation time with respect to the mid of the wire, assuming a propagation velocity of 0.244 m/ns, as directly measured with test-beam data [9].

These corrections should be modified in case of different running conditions. This is the case of cosmic data, where the previous definition of the TOF cannot be applied, or test-beam data, where the chamber is usually illuminated only in a small region. Particular care has been taken to provide adequate flexibility in the code.

In summary, the drift time is extracted from the TDC time by subtracting the t_0^{wire} of each wire, the $t_{\rm trig}^{SL}$ measured by the calibration procedure for each superlayer, which may account for the average TOF and time of signal propagation along the wire, and a further hit-by-hit correction for the latter two effects:

$$t_{\rm drift} = t_{\rm TDC} - t_0^{\rm wire} - t_{\rm trig}^{SL} - \Delta TOF - \Delta t_{\rm prop}. \quad (1)$$

The values from the test pulse calibration are expected to be determined with an uncertainty smaller than 0.5 ns. The $t_{\rm trig}$ pedestals may vary with the trigger conditions and in general the precision of their determination depends on the statistics of prompt muons accumulated in a given chamber, i.e. on the integrated luminosity of a given run. Typical accuraces of 1-2 ns are expected to be reached, thus giving a contribution of 50-100 μm to be added in quadrature to the intrinsic cell resolution.

This synchronization procedure can be applied also to simulated events. However, in the study of the hit reconstruction algorithms it is useful to decouple the performance of the algorithm itself from the resolution degradation introduced by the jitter of the measured synchronization constants. For this reason it is possible to use, during the reconstruction of simulated data, the time offsets determined during the digitization in place of the measured t_0 and $t_{\rm trig}$ pedestals. This is the case for the results presented in the following. The corresponding hit resolution is determined by the intrinsic cell resolution and by the precision on the corrections for TOF and signal propagation along the wire, but is not affected by uncertainties deriving from the calibration of the t_0 and $t_{\rm trig}$ pedestals.

4 Reconstruction of the Hit Position within the Cell

The primary result of the DT local reconstruction are points in the cell volume, also called "RecHits", which belong to the plane of the wires. These objects are built by computing the drift distance corresponding to the measured drift time.

Two reconstruction algorithms have been developed. The first assumes a constant drift velocity over the entire cell, an acceptable approximation thanks to the good cell linearity. The second is based on a time-to-distance parameterization obtained using a GARFIELD [10] simulation of the cell behavior, and takes into account the dependence of the drift velocity on the track incidence angle in the plane orthogonal to the wires and on the residual magnetic field [5], thus achieving better resolution. These two reconstruction algorithms are described in Sections 4.1 and 4.2, respectively.

As discussed in Section 3, corrections to the synchronization constants due to the TOF and the signal propagation along the wire have to be applied in order to achieve the best possible resolution. These corrections, as well as the parameters used as input for the cell parameterization (the track incidence angle and the magnetic field) cannot be computed for an individual digi, which only contains information about the hit distance from the wire. For this reason an iterative reconstruction procedure is adopted:

- *first step*: reconstruction at the cell level: the left-right ambiguity is unsolved and the position of the hit along the wire is not yet determined;
- *second step*: the hits are used to build a segment within a superlayer. The position along the wires is still unknown but the left-right ambiguity of each hit is solved. Also, the track impact angle is known, and this allows recomputing the hit positions more accurately if the cell parameterization is used;
- *third step*: the segments in r-ϕ and r-z projections are used to build a three-dimensional segment. The position of each hit along the wire is now fixed and can be used for a more precise estimation of the residual magnetic field, which varies along the tube affecting the drift velocity. Also the estimated delays due to the TOF and the signal propagation along the wire can be refined as discussed in Section 3, so that hit positions can be further improved.

In summary, the initial reconstruction at the cell level gives the input hits used to find a segment. When a segment is built, the position of its hits is further refined and the hits are then refitted.

In order to discard noise and pile-up signals, the reconstruction is performed only for drift times falling in a user-defined time window. The upper bound of this time window is normally set ≈ 25 ns above the maximum drift time in the cell (≈ 390 ns for a saturated drift velicity of 54 micron/ns) to conservatively take into account the effect of fluctuations and cell non-linearity on the time of arrival of the drifting electrons. Also, to avoid introducing

inefficiencies for very small drift times due to fluctuations in the arrival times and due to the precision of the t_0 and $t_{\rm trig}$ corrections, the time window is normally extended down to -3 ns. Times that after t_0 and $t_{\rm trig}$ subtraction are negative but lie within the acceptance window are associated to hits passing by the anode wire. All other digis are discarded as they cannot belong to the signal event which fired the trigger.

4.1 Reconstruction with Constant Drift Velocity

The good uniformity of the drift field within the cell allows reconstruction of the distance from the wire associated to a certain drift time under the assumption of a constant drift velocity ($v_{\rm drift}$) over the entire cell:

$$x = v_{\rm drift} \cdot t_{\rm drift}. \tag{2}$$

The drift velocity can be estimated from data with appropriate calibration procedures [8]. The same procedures also allow to estimate the error to be assigned to the reconstructed hits.

This simple reconstruction algorithm gives satisfactory results especially for tracks with small impact angles and in regions with low residual magnetic field, as in these cases the cell non-linearities are less important.

Although this method does not account for local variations of the magnetic field in the tube or for different impact angles of individual tracks, the calibration procedure determines by construction the average drift velocity which fits best the working conditions of the group of cells considered. Currently, the calibration is performed separately for each superlayer, so that the resulting drift velocity corresponds to the average conditions in each superlayer.

For this algorithm, the three-step reconstruction procedure described in Section 4 is only used for the refinement of the synchronization constants.

4.2 Reconstruction Using the Cell Parameterization

The optimal cell resolution can be achieved by taking into account the dependence of the drift velocity on magnetic field and track parameters, as the impact angle of the crossing track and the residual magnetic field in the gas volume affect the drift times. These effects are considered only on average for a group of cells by the algorithm described in the previous section, where the calibration cannot account for the non-linearities and the variation of the magnetic field along the tube.

An existing parameterization, obtained from a GARFIELD simulation [11], has been used to implement a reconstruction algorithm which computes the drift distance by considering its dependence on the track angle in the plane orthogonal to the wires (α) and on the components of the magnetic field parallel to the wire ($B_{\rm wire}$) and perpendicular to both the wire and to the drift direction ($B_{\rm norm}$).

This parameterization gives the distance from the anode of tracks that would give a drift electron arrival time distribution *peaked* at the given time $t_{\rm drift}$. We call this distance $x^{t_{\rm mode}}$ to indicate that it is the distance corresponding to a drift time distribution with the mode equal to $t_{\rm drift}$:

$$x^{t_{\rm mode}} = f(t_{\rm drift}, \alpha, B_{\rm wire}, B_{\rm norm}). \tag{3}$$

The parameterization also provides the sigma of the fit of the drift time distribution peaked at $t_{\rm drift}$ with two half Gaussians, on the left and on the right of the peak, converted to distances using the average drift velocity:

$$\sigma_p^x, \sigma_n^x = f(t_{\rm drift}, \alpha, B_{\rm wire}, B_{\rm norm}). \tag{4}$$

Actually, $x^{t_{\rm mode}}$ is not the relevant quantity for reconstruction, which requires the knowledge of the *average* distance from the wire for which the drift time is $t_{\rm drift}$. This is not available with the current parameterization. However, this quantity is approximately equal to the distance $x^{t_{\rm mean}}$ for which the drift time distribution has *mean* (instead than *mode*) equal to $t_{\rm drift}$. In the case of an ideal distribution composed of two half Gaussians, as considered by the parameterization, $x^{t_{\rm mean}}$ is related to $x^{t_{\rm mode}}$, σ_p^x and σ_n^x by:

$$x^{t_{\rm mean}} = x^{t_{\rm mode}} - (\sigma_p^x - \sigma_n^x)\sqrt{\frac{2}{\pi}}. \tag{5}$$

This is an approximation of the actual value. A more correct result could be obtained by a dedicated GARFIELD parameterization of the mean of the distribution of distances from the wire that result in a certain drift time. Such

a parameterization is currently not available. The effect of this approximation is expected to be small in all the regions of the cell where the width of the distribution is slowly varying along the cell axis. This is the case in the entire cell, except in the vicinity of the anode wire ($x^{t_{\rm mode}} \lesssim 1$ mm) where the discrepancy is anyhow below 50 μm.

The resulting parameterization has been implemented in the official CMS reconstruction code as a function of the form:

$$x_{\rm drift} = f(t_{\rm drift}, \alpha, B_{\rm wire}, B_{\rm norm}). \tag{6}$$

Since α, $B_{\rm wire}$ and $B_{\rm norm}$ are not known at the level of the individual hit, they are introduced during the three-step reconstruction procedure described in Section 4. For the first step, a crude estimate of the input parameters of the parameterization is used: the field value is taken at the middle of the wire and the track angles are determined assuming the track points to the the nominal interaction point. The hit is then updated twice: after having been used to build a two-dimensional r-ϕ or r-z segment (second step) and after having been included in a three-dimensional segment (third step).

At the second step the angle of the segment is used to update the RecHit position with Eq. 6. In the third step the knowledge of the hit position along the wire is used to better evaluate the magnetic field and $x_{\rm drift}$ is computed again. The knowledge of the three-dimensional position of the hit also allows refining the synchronization (cf. Section 3).

The quantities $\sigma_p^x(t)$ and $\sigma_n^x(t)$, that are available from the parametrization (Eq. 4), cannot be used to estimate the uncertainty to be assigned to the measurement. In fact, they represent the width of the drift electron arrival time distributions for a given hit position, translated into a distance, and not the spread of the position distribution that cosrresponds to a given drift time. The uncertainty on the reconstructed hit positions is therfore estimated from the residual distributions obtained subtracting the distances from the wire of RecHits and of the corresponding simulated GEANT hits. Gaussian fits have been performed and the corresponding sigmas recorded separately for r-ϕ and r-z superlayers for each reconstruction step. In the case of r-z superlayers, different uncertainties are assigned to the different wheels, as track impact angles in the plane orthogonal to the wires are larger for the external wheels. The uncertainty values for the different cases are reported in Table 1. At the third reconstruction step the uncertainty on the reconstructed distance is of the order of 200 μm for all the superlayer types in the different wheels. In this way, no dependence of the error on the hit position within the cell is taken into account.

Table 1: Uncertainties (in μm) assigned to one-dimensional RecHits reconstructed using the cell parameterization algorithm at the various reconstruction steps, for different types of superlayers and wheel positions. These uncertainties are obtained from a Gaussian fit of the residual distribution of the reconstructed drift distance on simulated events.

Superlayer type	r-ϕ	r-z, **Wheel** 0	r-z, **Wheel** ±1	r-z, **Wheel** ±2
Step 1	237	250	271	308
Step 2	231	250	271	305
Step 3	207	196	210	228

4.3 Performance of the Hit Reconstruction

The goal of this section is to show the algorithmic performance of the hit reconstruction on simulated data. The reconstruction is performed using the GARFIELD parameterization. The same $t_{\rm trig}$ offsets applied during the digitization are used for the synchronization, as discussed in Section 3. It should be noted once more that, while this choice allows decoupling the study of the reconstruction algorithm from the accuracy of the calibration procedure, the true cell resolution includes an additional contribution due to the accuracy in the computation of the t_0 and $t_{\rm trig}$ delays.

The simulated sample used for this study consists of 10^5 single muons generated with a flat p_T spectrum in the range 10–100 GeV/c, with $|\eta| < 1.3$.

The plots in Fig. 5 show the resolution on the (unsigned) distance from the wire for hits reconstructed in the DT cells of r-ϕ superlayers. The distributions are Gaussian, with the mean values and sigmas given in Table 2 separately for r-ϕ superlayers and for the r-z superlayers in the different wheels.

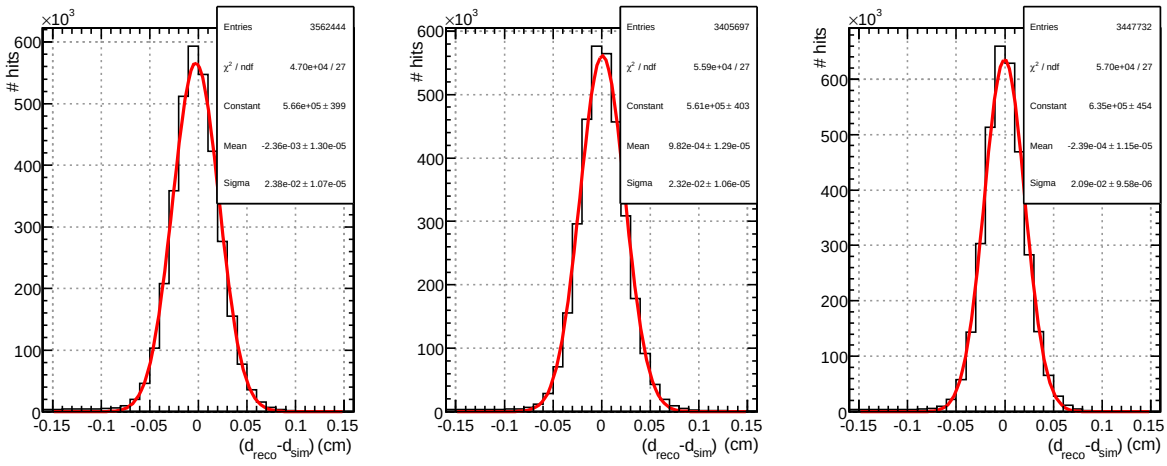

Figure 5: Residuals between the reconstructed and the simulated hit distances from the wire. The 3 plots refer to the first (left), second (center) and third (right) reconstruction step of the cell parameterization algorithm in r-ϕ superlayers.

Table 2: Residuals between the reconstructed and the simulated hit distances from the wire. The mean value (μm) and the sigma (μm) of the Gaussian fit are reported for the three reconstruction steps performed with the cell parameterization algorithm, in r-ϕ and r-z superlayers.

Superlayer type	r-ϕ		r-z, **Wheel** 0		r-z, **Wheel** ±1		r-z, **Wheel** ±2	
	mean	σ	mean	σ	mean	σ	mean	σ
Step 1	-23.6 ± 0.1	238	6 ± 0.5	265	6 ± 0.4	281	-7 ± 0.5	314
Step 2	9.8 ± 0.1	232	7 ± 0.5	264	7 ± 0.4	281	-4 ± 0.5	315
Step 3	-2.4 ± 0.1	210	-2.7 ± 0.4	204	-1.6 ± 0.5	219	-7 ± 0.4	231

The width of the residuals grows towards the outermost wheels in the r-z superlayers. This is due to the impact angle of muons, which increases with pseudorapidity, enhancing the effect of the cell non-linearities. This effect is less pronounced at the second and third reconstruction steps where the knowledge of the segment angle is used as input in the parameterization. The final resolution is about 200 μm in all the chambers.

The plots in Fig. 6 show the hit resolution as a function of the impact angle on the cell, using the parametrized algorithm, after each of the three steps described above. At the second step, the knowledge of the impact angle allows a better estimation of the effective drift velocity. The correction of this systematic effect improves the resolution for all angles.

The plots in Fig. 7 show the dependence of the hit resolution on the distance from the superlayer front-end. The incomplete correction for the signal propagation along the wire reflects into the dependence of the mean value with respect to the distance. The reconstruction at the third step fully compensates for this effect.

The tails of the residuals distributions are non-Gaussian and asymmetric as shown in Fig. 8, where the residuals after the first reconstruction step in r-ϕ superlayers are plotted. The long tail towards negative values is due to the delta-rays and secondary hits from electromagnetic debris. Due to the dead time of the TDC, only the hits giving drift times smaller than the one from the primary electron can be detected. The distribution drops sharply around 8.1 mm which, considering an average drift velocity of about 54 μm/ns, corresponds to the dead time of 150 ns set in the digitization.

The uncertainty assignment on the reconstructed position plays an important role in the segment reconstruction since the pattern recognition is based on a quality selection exploiting the χ^2 of the linear fit. The plots in Fig. 9 and 10 show the pull distributions for the three reconstruction steps in the r-ϕ and r-z superlayers, using for the reconstructed hits the errors given in Table 1. The parameters of the Gaussian fits of these distributions are given in Table 3.

The shape of the pull distributions is not perfectly Gaussian since the assignment of an uniform uncertainty along the whole cell is not the ideal choice due to the presence of critical regions, like the one close to the anode, where the drift time distribution is affected by strong non-linearities. This is visible for example in the plots of Fig. 11,

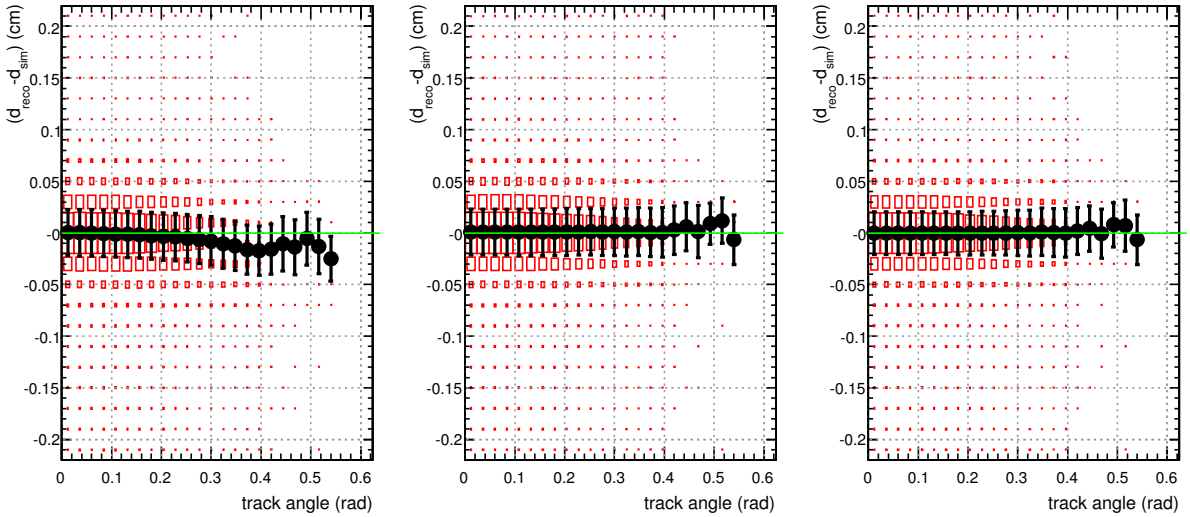

Figure 6: Residuals as a function of the impact angle on the DT cell after the first (left), second (center) and third (right) step of the hit reconstruction with the cell parameterization algorithm, for r-ϕ superlayers. The means and sigmas of a Gaussian fit for each histogram bin are shown.

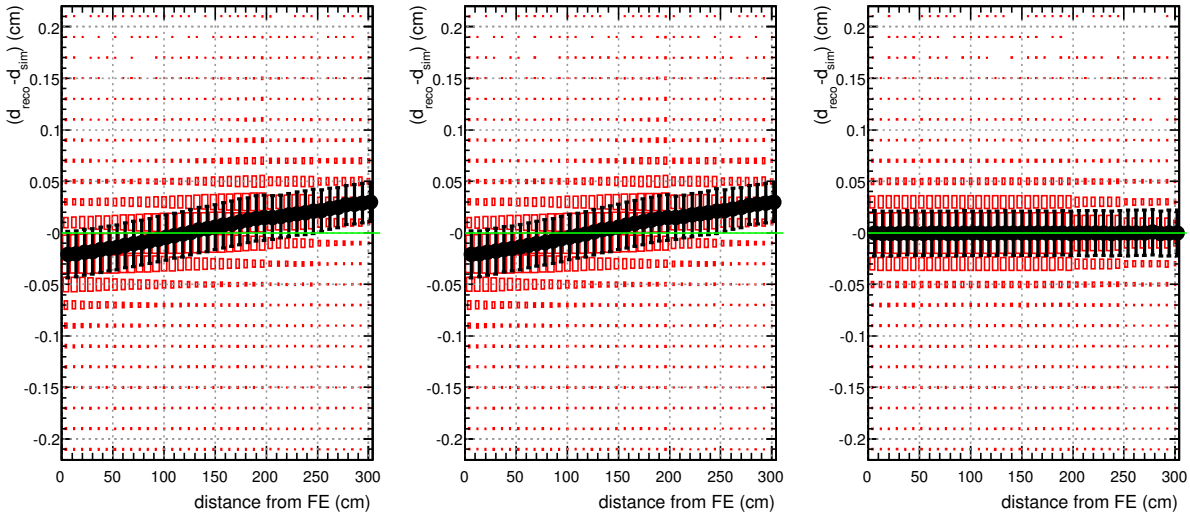

Figure 7: Residuals as a function of the hit distance from the front-end after the first (left), second (center) and third (right) step of the hit reconstruction with the cell parameterization algorithm, for r-z superlayers. The means and sigmas of a Gaussian fit for each histogram bin are shown.

which shows the pulls in r-z superlayers as a function of the distance from the anode. The widths of the pulls are however very close to unity in all the cases.

A comparison of the reconstruction algorithm with constant drift velocity (Section 4.1) with the algorithm based on the GARFIELD parameterization (Section 4.2) shows the effect of cell non-linearities. The plots in Fig. 12 show the residuals between the reconstructed and simulated distance from the wire as a function of the simulated one. They refer to the worst situation, the first reconstruction step in r-z superlayers of wheels $+2$ and -2, where the large impact angle and the non-negligible magnetic field enhance the effect of the non-linearities in the drift of electrons. The plot on the left shows the results obtained using the cell parameterization while the one on the right shows the performance of the constant drift velocity method. In the first case, the effect of the non-linearities is below 100 μm also in the most problematic region, close to the anode. The situation is completely different in the plot on the right where the average value of the residuals can vary by more than 150 μm when moving by a few millimeters away from the anode. It is evident that the correction of the non-linearity as a function of the distance from the wire can improve the accuracy beyond what can be achieved with a constant drift velocity assumption. It

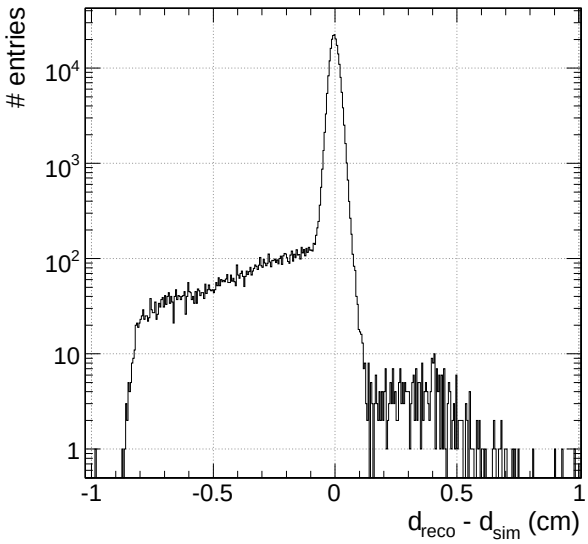

Figure 8: Residuals between the reconstructed and the simulated hit distances from the wire. The plot refers to the first reconstruction step performed with the cell parameterization algorithm, in r-ϕ superlayers. Note the extended range with respect to Fig. 5.

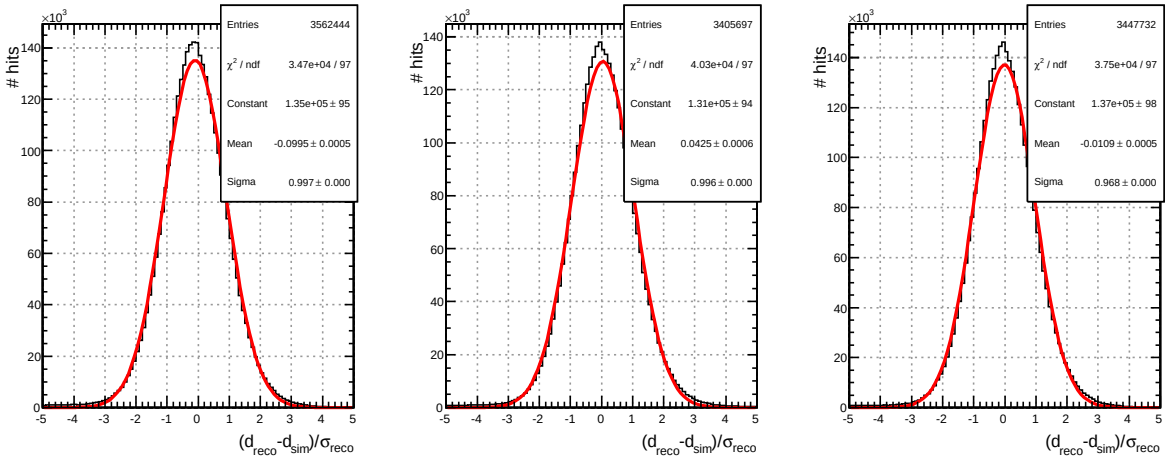

Figure 9: Pulls for the reconstructed distance from the wire. The 3 plots refer to the first (left), second (center) and third (right) reconstruction step of the cell parameterization in r-ϕ superlayers (all wheels).

must be noted, however, that in real life this improvement depends critically on the accuracy of the determination of the $t_{\rm trig}$ corrections and of the input parameters of the parametrization (e.g. of the magnetic field in the region of the hit), besides depending on the accuracy of the parametrization itself. Specific validation on real data will therefore be mandatory before adopting this algorithm.

5 Segment Reconstruction

Under ideal circumstances, a muon coming from the interaction region gives twelve hits in a chamber, one in each layer. In practice some hits may be missing due to inefficiencies; tracks at large angle may give rise to two hits in adjacent cells of the same layer and there may be additional hits due to background from electromagnetic debris, neutrons and noise. The purpose of the segment building procedure is to identify which of the reconstructed hits stem from the muon track to reduce the combinatorics, to resolve the left-right ambiguity for each of the hits and to provide a position and direction estimate for the track crossing the chamber. Moreover, the combined use of many hits also allows an increase in the spatial resolution for individual hits, as the segment reconstruction provides a precise determination of the track impact angle and of the hit position along the wire, which can be used to refine the computation of the drift distance (cf. Section 4).

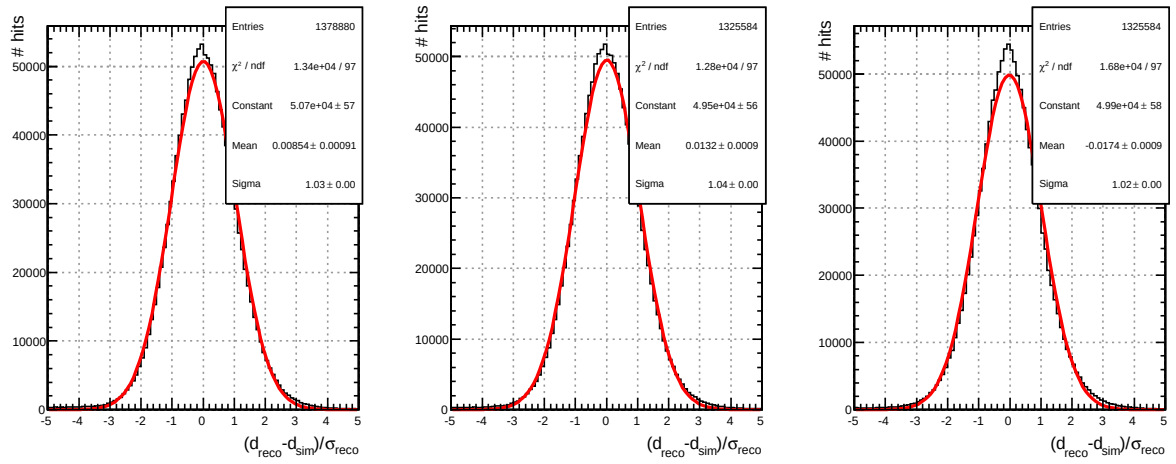

Figure 10: Same as for Fig. 9, for superlayers r-z (all wheels).

Table 3: Pulls of the reconstructed distance from the wire. The sigmas of the Gaussian fit are given for the three reconstruction steps performed with the cell parameterization algorithm in r-ϕ and r-z superlayers.

Superlayer type	r-ϕ	r-z, **Wheel** 0	r-z, **Wheel** ±1	r-z, **Wheel** ±2
Step 1	0.997	1.053	1.030	1.015
Step 2	0.996	1.050	1.031	1.027
Step 3	0.968	1.031	1.031	1.004

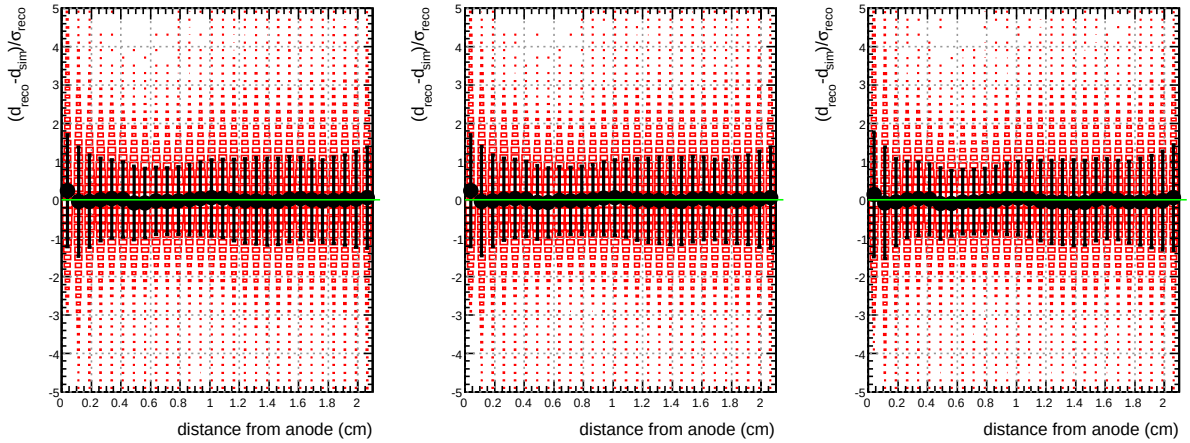

Figure 11: Pulls for reconstructed hits as a function of the distance of the hit from the anode wire. The 3 plots refer to the first (left) second (center) and third (right) reconstruction step of the cell parameterization algorithm in r-z superlayers.

The segment reconstruction acts in each chamber on the r-ϕ and r-z projections independently: only at the end of the procedure the two projections are combined and a three-dimensional segment is built [1)].

The reconstruction in each projection is an exercise of pattern recognition and fitting, with the complication of left-right ambiguity. A linear fitting model, given the hit resolution and the small height of a chamber, is adequate. The reconstruction is performed in three steps:

- segment candidates are built from sets of aligned hits;
- the best segments among those sharing hits are selected, solving conflicts and suppressing ghosts;

[1)] In the CMS jargon, a segment in one projection is referred to as "2D-segment", meaning that it provides 2 measurements: the position and the track angle in one projection. Likewise, a segment in space, built using two projections, is called "4D-segment", since it provides 4 parameters (2 positions and 2 angles).

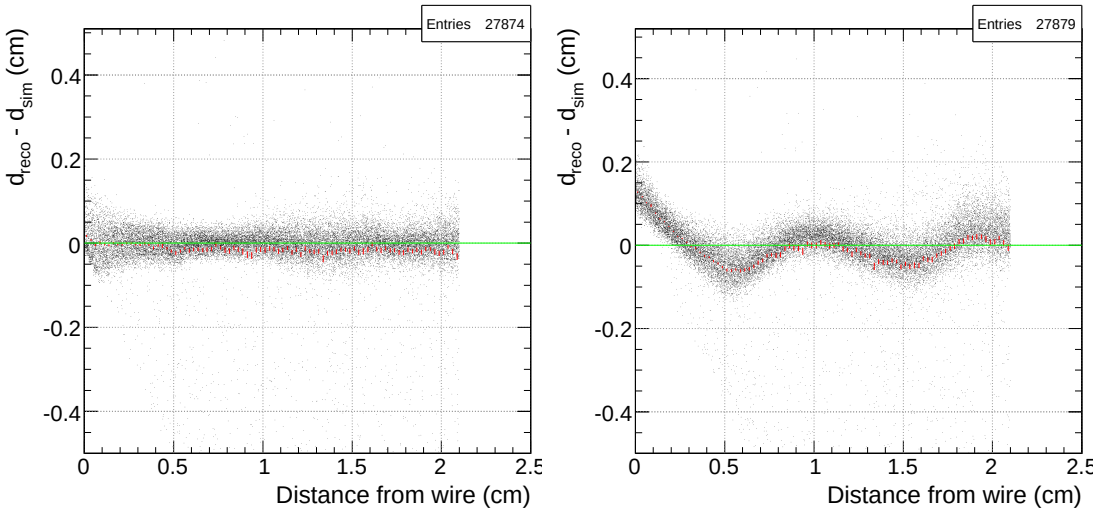

Figure 12: Residuals between the reconstructed and simulated distance from the wire as a function of the simulated one. The plots are referred to hits reconstructed using the cell parameterization algorithm (left) and the constant drift velocity algorithm (right) in r-z superlayers of wheels ± 2.

- the position of the used hits is then updated using the information from the segment (cf. Section 4) and the segments themselves are eventually re-fitted.

Building segment candidates. The first step begins by selecting pairs of hits in different layers, starting from the most far away layers. For each pair the reconstruction of a segment candidate is then attempted.

A pair is kept if the angle of the corresponding proto-segment is compatible with a track pointing to the nominal interaction point within a given tolerance, usually set to 0.1 rad for the r-z projection and 1.0 rad for the r-ϕ one, since this is the projection where the track bending occurs. These constraints can be switched off for the reconstruction of cosmic muons. As each hit has a left-right ambiguity, both hypotheses are considered, provided they fulfill the above condition.

For each pair, additional hits are searched for in all layers. Hits are considered when distance from the extrapolated segment is smaller than 10 times the position error, as estimated by the hit-building algorithm. It is possible that both the left and right hypotheses are compatible with the segment. In this case, both candidates are retained and the ambiguity is solved later. Also, a muon can cross the I-beam separating two cells generating a signal in both. In this case, both hits are considered for that layer, in order to avoid any bias.

Once the pattern recognition is completed, each collection of hits is fitted. For each seed (i.e. pair of hits) only the segment candidate with the maximum number of hits is retained. Among all candidates with the same number of hits, that with lowest χ^2 is chosen. Only segments with at least three hits and $\chi^2/\text{d.o.f.} < 20$ are accepted.

This algorithm is applied directly to the r-z superlayer in each chamber. It can also be applied to individual r-ϕ superlayers, and the resulting segments are useful for commissioning and studies of superlayer performances. However, for the purpose of track fitting it is more convenient to consider the two r-ϕ superlayers in a chamber together. The procedure described above is therefore applied to the eight r-ϕ layers of each chamber and the resulting segments are then used for building three-dimensional segments, as described in the following.

In case of showering, the occupancy in the chamber can be extremely high. Pattern recognition is critical in this case, first because hits from secondary particles may mask the true muon hits if they happen to be closer to the wire, due to the cell dead time; and second because high occupancies lead to large combinatorics which can deteriorate the performance of the pattern recognition. For this reason the procedure described above is not attempted if the number of hits in either the r-z or the two r-ϕ layers is larger than a programmable number (default is 50). According to MonteCarlo studies, a 100 GeV muon has a probability of about ~ 0.03 % to leave more than 50 hits in a DT chamber (~ 0.15 % for > 30 hits), while the probability increases to 1.2 % and 3.0 % for a threshold of 50 and 30 hits, respectively, for a 1 TeV muon. Given the presence of 4 stations, the effect of skipping the segment reconstruction in case of large occupancies is small. A clustering algorithm, designed to allow the reconstruction the centroid of the shower, is being developed.

Segment selection. The pattern recognition described above produces a set of segment candidates. A consistency check is performed in order to test whether two candidates use different left-right hypotheses for the same hit. In this case, the conflicting hit is removed from the worse of the two segments, where quality is defined, as above, by the maximum number of hits and the minimum χ^2.

Specific incidence angles can result in hit patterns for which two segment candidates share all their hits, with different left-right hypotheses for each one. The two candidates have in this case the same quality. In p–p collisions, the choice is implicit in the request of compatibility with the nominal interaction point described previously. When this requirement is removed, as for the reconstruction of cosmic muons, two options are available: either retaining both candidates, thus leaving the selection of the best segment to the muon track fit algorithm, or choosing the candidate with the smallest angle (with respect to the chamber vertical) among the conflicting ones, which in specific operating conditions is most likely to be the correct choice.

The segments are allowed to share non-conflicting hits up to a given number: the default is two. If more are present, the worst candidate is rejected. If two segments share some hits, they are required to have a minimum number of non-shared hits, in order to further reduce the number of short ghost segments. The minimum number of non-shared hits is programmable as well and the default is two.

The hits from the remaining candidates are updated ("second step" mentioned in Section 4.2), taking into account the incidence angle reconstructed by the segment. The segment linear fit is then recomputed using the updated hits.

Matching of the two projections. Up to this point, the r-ϕ and r-z projections are handled independently. As the two projections are orthogonal, a segment in one projection cannot be used to validate a segment in the other: all combinations of segments from the two projections are kept.

The additional knowledge of the hit position along the wire is used to update the x position in the cells ("third step" described Section 4.2) before performing the final fit of the segment. The result is a segment inside a chamber suitable for use in the track reconstruction.

5.1 Performance of the Segment Reconstruction

5.1.1 Angle and Position Residuals of the Segments

Position and angle residuals for two-dimensional segments on a single superlayer are shown in Fig. 13 and 14 for r-ϕ and r-z projections, respectively. The position resolutions are about 115 μm and 140 μm in the two cases. The worse resolution on the r-z projection is mainly due to the higher impact angle of the muon in these superlayers. The resolution on the angle is about 8 mrad for both projections. It is worth to stress that, in the r-ϕ projection, segments built using both r-ϕ superlayers are used.

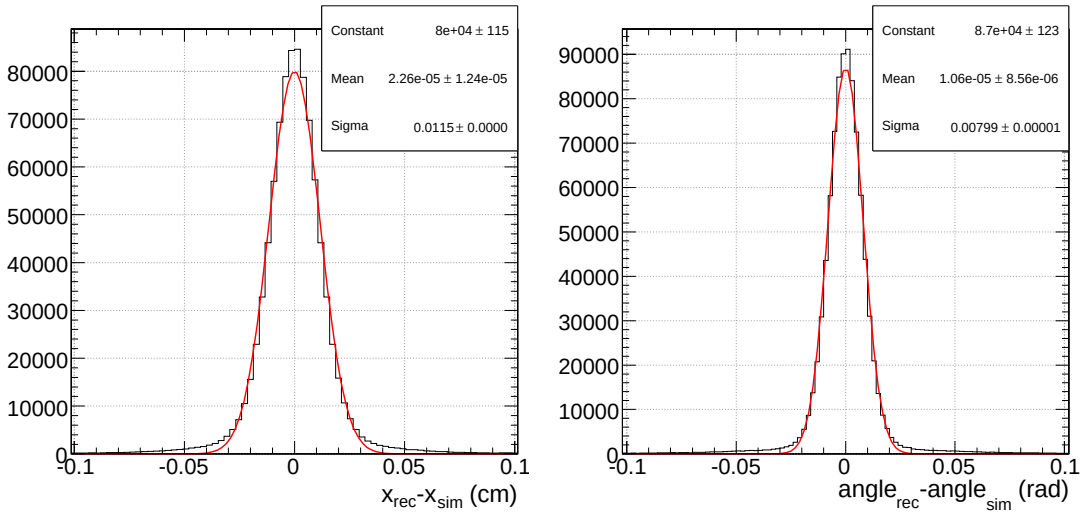

Figure 13: Residuals on the position (left) and angle (right) measured by two-dimensional segments in individual r-ϕ superlayers.

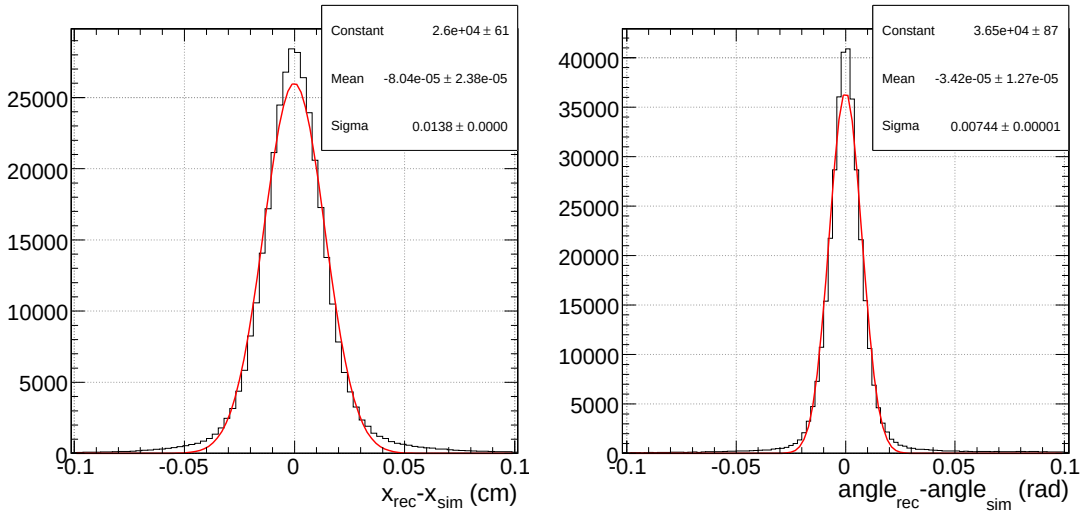

Figure 14: Residuals on the position (left) and angle (right) measured by two-dimensional segments in r-z superlayers.

The three-dimensional segments built by combining the r-ϕ and r-z projections are the basic ingredient for the track fit. Figure 15 shows the residuals on the bending coordinate x and on the non-bending coordinate y, which are the components measured by the r-ϕ and r-z superlayers, respectively. The resolution improvement with respect to Fig. 13 is due, in the case of x, to the fact that the two r-ϕ superlayers are now used together, thus doubling the number of measurement planes and increasing the lever arm from ≈ 4 cm to ≈ 25 cm. Also, for both projections the single hit resolution is better due to the additional knowledge of the position of the hit along the wire. In the

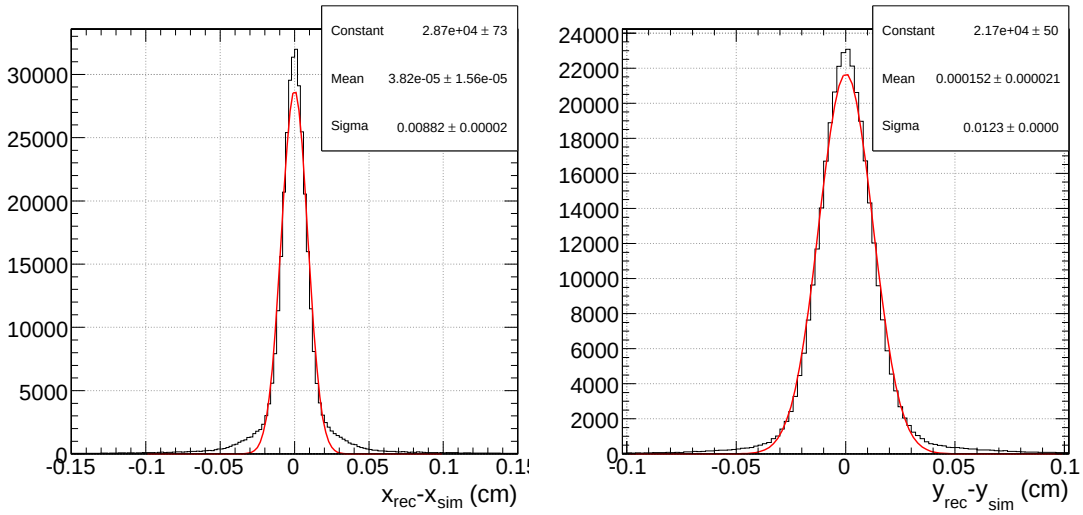

Figure 15: Residuals on the position of three-dimensional segments. Left: residual on x (bending coordinate), given at the middle plane of the two r-ϕ superlayers. Right: residual on y (non-bending coordinate) given at the middle plane of the r-z superlayer.

bending plane, with a resolution of about 240 μm for the single one-dimensional hit (see Section 4.3), it is possible to achieve a precision of about 90 μm. Moreover, spurious hits are rejected and the combinatorics for the next reconstruction steps is reduced.

The resolution on the non-bending coordinate is about 120 μm. The most accurate determination of a segment coordinate is obtained at a plane corresponding to the center of gravity of the hits, weighted by their errors. This corresponds approximately to the middle plane of the chamber in the case of the r-ϕ projection, and the middle plane of the r-z superlayer for the r-z projection. These two planes do not coincide, as can be observed in Fig. 3. However, it is often convenient to give the position of the segment as a single three-dimensional point, and in this case both coordinates have to be given at the same plane. The middle plane of the chamber is chosen, in order to favor the bending coordinate, while the non-bending coordinate has to be extrapolated from the position measured

on the middle plane of the r-z superlayer. Therefore in the 3D position of the segment, the residual on the y coordinate is degradated to about 530 μm (the full error matrix, including the correlations terms between positions and angles, is available). If a precise estimate of the position of the segment in the non-bending coordinate is required, it is recommended to use the position of the r-z segment projection defined in the r-z superlayer frame rather than the y coordinate of the 3D segment position.

The resolution on the direction of the reconstructed segments is shown in Fig. 16. An angular resolution of about 0.7 mrad is achieved in the r-ϕ projection, thanks to the presence of two superlayers with a long lever arm. On the other projection (r-z), the resolution is about 6 mrad.

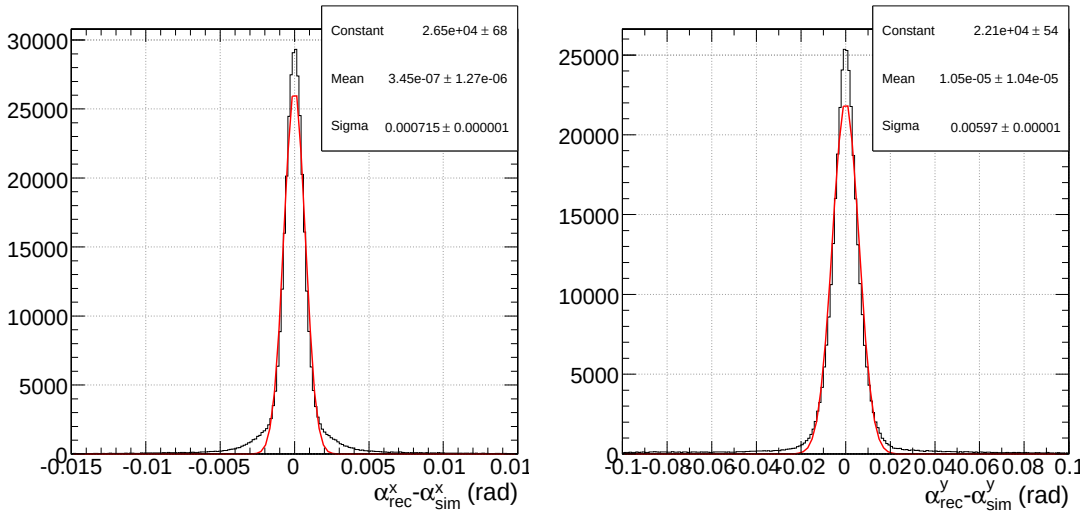

Figure 16: Residuals on the angles measured by three-dimensional segments in the r-ϕ (left) and r-z (right) projections.

The large non-Gaussian tails of the distribution are mainly due to the presence of energetic secondary hits which, crossing different layers, can affect the pattern recognition.

In Fig. 17, the pulls for the three-dimensional segments are shown. The pulls are well centered at zero and with a σ close to unity. No dependence of the pull on η is present, as shown in Fig. 18.

6 Conclusions

We have summarized the algorithms currently implemented in the CMSSW software for the local reconstruction in the DT system of CMS.

Concerning the resolution, the GARFIELD parameterization used in the reconstruction of the hits gives better results with respect to the constant drift velocity, especially in the most critical regions, thanks to the modeling of the cell non-linearities and the fact that it can take into account the dependence of the drift velocity on the residual magnetic field. In particular the parametrization accounts for the variation of the magnetic field along the wire, which can be significant especially in the outermost wheels and cannot easily be accounted for with the linear drift velocity algorithm. However, the reconstruction algorithm based on the parameterization of the cell behavior is more complex than the one using a constant drift velocity. This suggests caution in exploiting it at the start-up of LHC. The constant drift velocity algorithm, with average drift velocity measured from data, is a safe choice to be used with the first collision data and can provide adequate accuracy while a full validation of the parametrization on real data is developed. A comparison of the performance of the two algorithms on real data is not in the scope of the present document. Studies on test-beam data are described in [12].

Moreover, the parameterization of the cell is still open to further improvements. In fact, the parameterization currently used was not designed for the reconstruction: a more detailed treatment would require a dedicated GARFIELD simulation. In particular the simulation should be used to build the distribution of the distances corresponding to a certain drift time, extracting from that a parameterization of the average drift-distance and of the width of the distribution which would allow parameterizing also the error associated to the reconstructed hit.

As far as segment building is concerned, the problem of high occupancy in the presence of muon showering should be addressed with a dedicated reconstruction not based on the current combinatorial pattern recognition. A possible

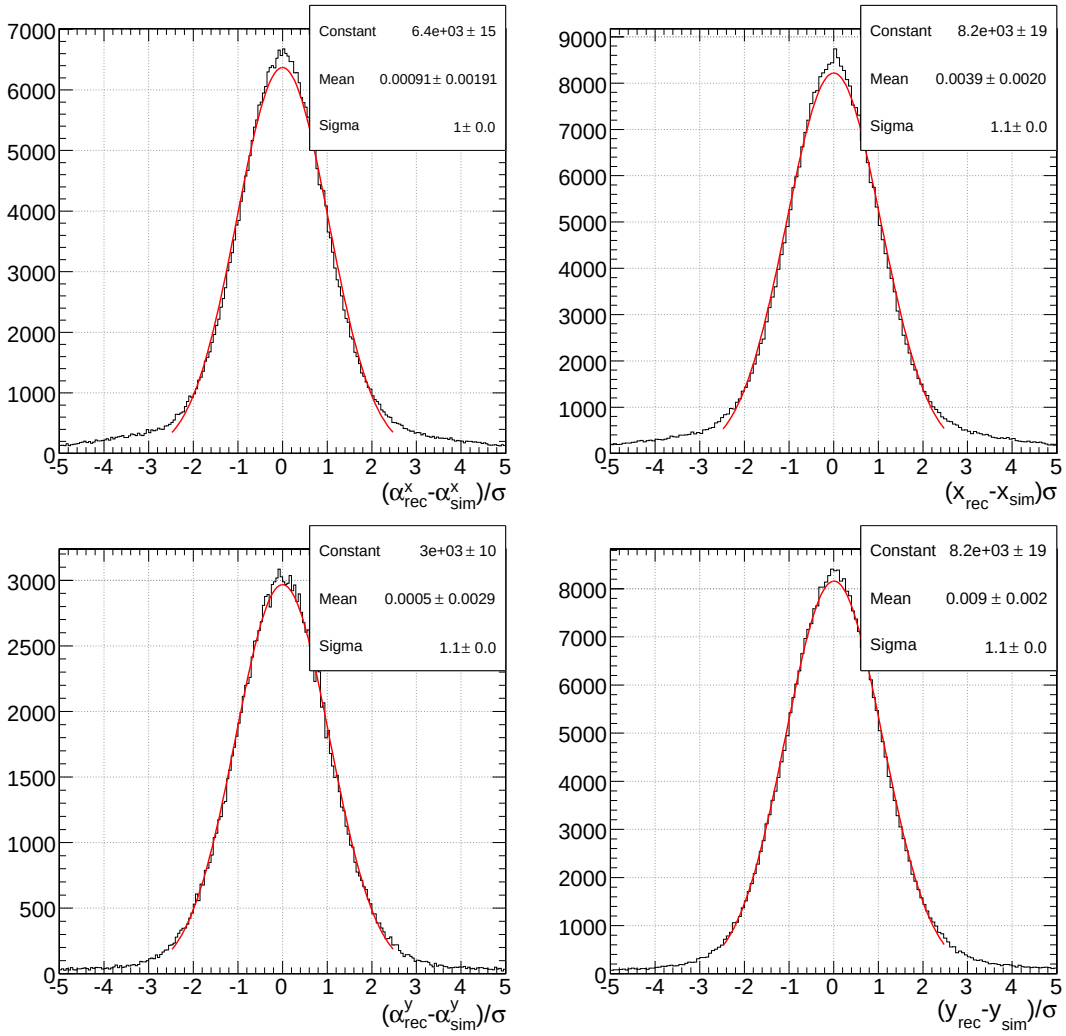

Figure 17: Pulls on the parameters measured by three-dimensional segments. Top line: pulls for angle (left) and position (right) in the r-ϕ projection. Bottom line: pulls for the r-z projection, given at the middle plane of the r-z superlayer (see text).

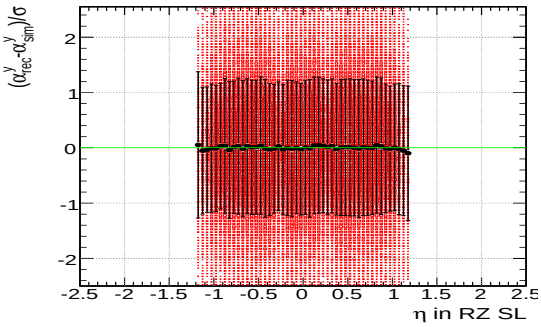

Figure 18: Pull on the angle in the r-z projection vs η . The black dots show the mean and the bars the sigma of Gaussian fits on each η slice.

solution which is under study is a clustering algorithm of the hits in the chamber; this would allow skipping the segment building when the hit multiplicity is too high.

It is worth noticing that the local reconstruction procedure has been designed for p–p events, namely for bunched muons coming from the interaction point. However, since October 2005 the reconstruction has been extensively used also for cosmic events during the chamber commissioning, the Cosmic Challenge and all subsequent cosmic data taking, both in the offline analysis of the data and in the on-line monitoring of the data quality.

The tests of the reconstruction on real data have been extremely useful for the whole reconstruction chain, leading also to many improvements in its design. The algorithms described here have shown enough flexibility to treat data acquired in different running conditions: cosmics, test-beam and simulated p–p data, allowing different treatment of calibration, synchronization constants and tuning of the algorithms.

References

[1] C. D. Jones et al., *The New CMS Data Model and Framework*, Proceedings of the Conference on Computing in High Energy Physics, Mumbai (2006).

[2] The CMS Collaboration, *Technical Proposal*, CERN/LHCC 94-38, LHCC/P1 (1994).

[3] The CMS Collaboration, *The Muon Project, Technical Design Report*, CERN/LHCC 97-32, CMS TDR 3 (1997).

[4] The CMS Collaboration, *CMS Physics: Technical Design Report. Volume I: Detector Performance and Software*, CERN/LHCC 2006-01, CMS TDR 8.1 (2006).

[5] M. Aguilar-Benítez et al. , *"Construction and test of the final CMS Barrel Drift Tube Muon Chamber prototype"*, Nucl. Inst. & Meth. **A480** (2002) 658.

[6] F. Gasparini et al., *Bunch Crossing Identification at LHC Using a Mean-timer Technique*, Nucl. Inst. & Meth. **A336** (1993) 91.

[7] P. Arce et al., *Bunched beam test of the CMS drift tubes local muon trigger*, Nucl. Inst. & Meth. **A534** (2004) 441.

[8] N. Amapane et al., *Offline Calibration Procedure of the Drift Tube Detectors*, CMS Note **2007/034** (2007).

[9] F. Cavallo et al., *Test of MB3 Muon Barrel Drift Chamber with Cosmic Rays*, CMS Note **2003/017** (2003).

[10] R. Veenhof, *Garfield, a Drift-Chamber Simulation Program user's guide*, CERN Program Library W5050 (1994).

[11] J. Puerta-Pelayo, M. C. Fouz and P. Garcia-Abia, *Parametrization of the Response of the Muon Barrel Drift Tubes*, CMS Note **2005/018** (2005).

[12] U. Gasparini et al., *Comparison of DT Testbeam Results on Local Track Reconstruction with the OSCAR + ORCA Simulation*, CMS Note **2006/009** (2006).